Chapter 4

Generation of Baryon Inhomogeneity by Cosmic String Wakes

4.1 Introduction

We have discussed the model of ref.[14] in §3.4.2, where it was shown that the cosmic string induced density fluctuations can affect the quark-hadron transition in an important ways, and can lead to formation of extended planar regions of baryon inhomogeneities. However, in their study, the authors considered the density fluctuations produced by *straight* strings only and then discussed it's effects on quark-hadron transition. However, simulations [77] of the string network in the expanding universe show that the long cosmic strings possess substantial amount of small scale *wiggly* structures running along the strings. In proper treatment, one should take into account the effect of these wiggles on the shock formation, and consequently, on the resulting density fluctuations. However, as we see below, the qualitative picture will remain same, even in the presence of the wiggles along the long strings. Also, as we are interested only in the order of magnitude estimate of the baryon inhomogeneities

generated in the model of ref.[14], for simplicity, we will present our analysis for the case of straight strings only. However, for the sake of completeness, we will spend a bit to discuss this topic in the following section, and then our main analysis on baryon inhomogeneities generation will be presented in the next section. As we find below, the magnitude and length scale of these inhomogeneities are such that, they should survive indeed (as was expected by the authors of ref.[14]) until the stage of nucleosynthesis.

4.2 Density Fluctuations Produced by "Wiggly" Cosmic Strings

The presence of wiggles along the strings effectively increase the average energy density of the string and makes the strings to move slower. For physics at large scales (compared to the scale of wiggles l_w, which is expected to be set by the gravitational-radiation from the string [78] and given as, $l_w \simeq \Gamma G\mu t$ where μ is the mass per unit length for unperturbed string, Γ is a numerical factor of order 100), the effect of wiggles is taken into account by defining the effective mass per unit length μ_w and the string tension T_w. Unlike the case of straight string (as we described in §2.3.1 & §3.4.1), these quantities for perturbed string are not equal and they are related by the equation of state [78], $\mu_w T_w = \mu^2$. Because of the presence of these small scale structure, the static wiggly strings develop Newtonian gravitational field and a test particle at rest with respect to such perturbed string experiences attractive gravitational force. The metric around the wiggly string and density structure of the wake for collisionless particles have been studied and discussed in the literatures [6, 50, 78]. It turns out that, for moving wiggly string, total impulsive velocity imparted on the particles towards the surface swept out by the string is given as [78],

$$v_{impul} = 4\pi G\mu_w v_{st}\gamma_{st} + \frac{2\pi G(\mu_w - T_w)}{v_{st}\gamma_{st}}. \tag{4.1}$$

Where, first term is the usual velocity impulse arises due to the conical structure of the space-time around the wiggly string, with μ being replaced by the effective mass per unit length μ_w. The second term arises due to the Newtonian gravitational field developed by the wiggliness of the string. Using the value of $\mu_w \sim 1.9\mu$ and $T_w \sim 0.5\mu$ (see ref.[6]), we see from Eq.(4.1), if the string moves with ultrarelativistic speed, then the first term will dominate over the gravitational term. The rms velocity of the wiggly string on the scale of smallest wiggles found out to be, [79] $v_{st} \sim 0.6$. For this case, gravitational term can be neglected. In this case, density fluctuations for collisionless particles will be order of unity with opening angle, $\theta_w \simeq 8\pi G\mu_w$ (see Eq.(3.11). However, the velocity of the string obtained by taking average over a correlation length comes out to be very small ($v_{st} \sim 0.15$) for which gravitational effect should be taken into account.

Formation of density structure of wake for collisionless particles have been studied in ref.[78] assuming the particles remain at a distance far from the string and the particles will experience only averaged effect of the wiggles (in this case, relevant velocity is, $v_{st} \sim 0.15$). In the string rest frame (string lying along z-axis), if the particles moves with velocity v_{st} in the (+ve) x direction, then following ref.[78], resulting density fluctuations can be written as,

$$(\frac{\delta\rho}{\rho}) \simeq 1 + 4G(\mu_w - T_w)(\frac{1 - v_{st}^2}{v_{st}^2})(\frac{x - X_0}{X_0}). \tag{4.2}$$

Where, X_0 is of order of the inter-string separation. Note, setting the second term equal to zero, one recovers the result for density structure of the wake for straight string. If we put the value of wiggly string parameter in Eq.(4.2), we see that order of magnitude of density fluctuations will not be affected compared to the case of straight string (Eq.(3.11)).

Now, we discuss the effect of wiggliness on the value of density fluctuations produced by moving string through the relativistic fluid. Study on formation of shock by moving wiggly string has been done in the work of ref.[78] under some simplifying

assumptions. In their study, authors have treated the fluid as a non-viscous, non-relativistic fluid. As has been argued in ref.[78], the assumptions of non-relativistic fluid can be good approximation for the string velocity $v_{st} \sim 0.2$ which is relevant for the distance scale larger than the scale of the wiggles. Formation of wakes for wiggly strings has been discussed in ref.[78] after recombination. It is also mentioned in ref.[78] that similar wake should arise due to wiggly string even at earlier stages, when string moves through the relativistic plasma, even with $v_{st} = 0.15$ for the wiggly string. If we follow the approach of refs.[72, 73, 74], then $v_{st} = 0.15$ is subsonic and no shock can form. However, this does not represent the actual physical situation. This is because at smaller distance scales (compared to the scale of the wiggles), the straight segments of the string move with $v_{st} \simeq 0.6$ (ref.[79]). This is supersonic motion and shock will form. Because of the random velocities of different segments of the string, the individual shocks will combine to give some resultant shock and hence, wake for the total length of the (wiggly) string. Thus we can assume that even with the wiggles, shock and wake formation results. For these wakes, one can use Eq.(3.19) with $v_{st} = 0.6$ and mass per unit length μ for the straight string (as individual segments are straight). However, now the length scale of the shock (wake) will be governed by the size of each straight segment. The length of the wake (in the direction away from the string) will still be governed by the average inter-string separation. That will not be affected by the presence of the wiggles. (Recently, the evolution of wiggly string network has been studied [6] on flat space-time. The results suggest that even in the presence of wiggles the string network obey scaling solution. Authors in ref.[6] also mentioned that the average inter-string separation also scales with time. Though above simulation has been done on flat space-time, the author believes that such scaling solution is expected to exhibit in expanding universe also. If this is the case, then on an average inter-string separation for long wiggly string will not be altered from the straight string case.) However, the width of the wake (along the string direction) will now be truncated down to the average size of individual straight segment. Note however that, this simply changes the geometry of a

planar wake (for a completely straight string) to a collection of strips with each strip corresponding to individual straight segment of the wiggly string. Even the geometry of these strips may not be planar due to rapidly changing velocity of string segments. For a correct treatment, one should properly account for the different velocity and orientations of these strips. However, in this thesis, we we will ignore these complications. Following Eq.(3.19), the opening angle of the wake and density fluctuation for each straight segment of the wiggly string can now be written as (using $v_{st} = 0.6$ and sound velocity $v_s = 1/\sqrt{3}$),

$$\theta_w \simeq 70^0, \qquad \delta\rho/\rho \simeq 4 \times 10^{-5}. \tag{4.3}$$

Note that, the opening angle of the wake is somewhat larger than that of straight string case, Eq.(3.20). However, as the individual shock will combine to give resultant shock, we expect that the overall volume of the wakes will remain same (upto some factor of order one) as for straight string case. Therefore, in the following analysis for determining the baryon inhomogeneities, we will focus on the straight string case only.

4.3 Density Profile of Baryon Inhomogeneities

To determine the detailed profile of the baryon inhomogeneity resulting from the picture described in §3.4.2, we have to calculate the evolution of baryon densities in the QGP phase and in the hadron phase as the transition proceeds. (Note, the starting point of our analysis is to consider the universe as has already entered into the slow combustion phase. This slow combustion phase, in the presence of density fluctuation already has been discussed in §3.4.2. During this slow combustion phase, the transition proceeds through the collapsing of the interfaces, which separate the QGP phase inside the wake and the hadron phase outside.) First, we note that typical separation between string wakes (and hence resulting baryonic sheets) will be governed by the number of long strings in a given horizon, which is expected to be

about 15 (from numerical simulations [79]). The exact structure of these wakes in a given horizon volume needs to be known in order to study the concentration of baryons by advancing interfaces as the transition to hadronic phase proceeds. For example, if the string wakes are reasonably parallel, then they will span most of the horizon volume, as the average thickness of a wake (with parameters in Eq.(3.20) will be order 1-2 km (a single string wake will not be expected to extend over the entire horizon). In such a situation, the hadronic phase will first appear in the regions between the wakes, which may cover a very small fraction of the horizon volume initially. The initial value of the fraction f of the QGP phase to the hadronic phase will then be close to 1. f will then slowly decrease to zero as the planar interfaces (formed by the coalescence of bubbles in the region in between the overdense wakes) move inward, converting the QGP region inside the wake into the hadronic phase. Certainly, the actual situation will be more complicated than this, with string wakes extending in random directions, and often even overlapping. In such a situation, even the initial value of f, when bubble coalescence (in the regions between the wakes) forming planar interfaces, may be smaller than 1 (though not much smaller). However, again, this does not affect the order of magnitude estimate of the profile of the resulting baryon inhomogeneity as we determine below. Therefore, we use a simple picture, by focusing on the region relevant for only one string, covering about 1/15 of the horizon volume. Further, we take the initial value of f to be almost 1.

The baryon evolution in this overdense wake region and outside of this region will depend on the detailed dynamics of the phase boundary and the expansion of the universe during this epoch. To study this we will follow the calculations of Fuller et. al.[64] who have studied the evolution of the baryon fluctuations which might have been produced at the end of nucleation epoch during the QCD phase transition. In ref.[64], the evolution of baryon density in the QGP phase and in the hadron phase has been calculated as the hadronic region expands at the cost of the volume of the QGP phase during the co-existence temperature epoch. The main difference between their model and the model described in §3.4.2 is that, the QGP regions of interest

for them are expected to be spherical, while for the later case, it is a thick sheet-like region, with planar interfaces separating the QGP region from the hadronic region.

Let us first recall the effect of the expansion of the Universe on the dynamics of the phase transition [14, 64]. If $R(t)$ is the scale factor of Robertson-Walker metric, then Einstein's equations give [14, 64],

$$\frac{\dot{R}(t)}{R(t)} = \sqrt{\frac{8\pi G\rho(t)}{3}}. \tag{4.4}$$

Where ρ is the average energy density of the mixed phase. The energy density, entropy density, and pressure (ρ_q, s_q, p_q) in the QGP phase and (ρ_h, s_h, p_h) in the hadronic phase are,

$$\rho_q = g_q aT^4 + B,\ s_q = \frac{4}{3}g_q aT^3,\ p_q = \frac{g_q}{3}aT^4 - B \tag{4.5}$$

$$\rho_h = g_h aT^4,\ s_h = \frac{4}{3}g_h aT^3,\ p_h = \frac{g_h}{3}aT^4. \tag{4.6}$$

Here $g_q \simeq 51$ and $g_h \simeq 17$ are the degrees of freedom relevant for the two phases respectively (taking two massless quark flavors in the QGP phase, and counting other light particles) [64] and $a = \frac{\pi^2}{30}$. At the transition temperature we have $p_q = p_h$ which relates T_c and the bag constant B as, $B = \frac{1}{3}aT_c^4(g_q - g_h)$. We define $x = g_q/g_h$ to be the ratio of degrees of freedom between the two phases. For the mixed phase, we write the average value of energy density as, $\rho = f\rho_q + (1-f)\rho_h$. Here f denotes the fraction of the volume in the QGP phase. With this, Eq.(4.4) can be written as,

$$\frac{\dot{R}(t)}{R(t)} = (\frac{8\pi GB}{3})^{1/2}[4f + \frac{3}{x-1}]^{\frac{1}{2}}. \tag{4.7}$$

Now, conservation of the energy-momentum tensor gives,

$$R(t)^3\frac{dp(t)}{dt} = \frac{d}{dt}\{R(t)^3[\rho(t) + p(t)]\}. \tag{4.8}$$

During the transition, T and p are approximately constant. With this, Eq.(4.8) can be rewritten as,

$$\frac{\dot{R}(t)}{R(t)} = -\frac{\dot{f}(x-1)}{3f(x-1)+3}. \tag{4.9}$$

Eq.(4.7) and Eq.(4.9) along with the transport rate equations, which will be discussed bellow, will give the evolution of baryon densities in the quark gluon plasma phase and in the hadron phase. The evolution of baryon density can be studied in each phase as the interfaces move forward and baryons are transported from one phase to another. If n_b^q and n_b^h are the net baryon densities in the QGP phase and the hadron phase respectively, then their evolution equations are as follows [64]

$$\dot{n}_b^q = -n_b^q\lambda_q + n_b^h\lambda_h - n_b^q[\frac{\dot{V}(t)}{V(t)} + \frac{\dot{f}}{f}], \tag{4.10}$$

$$\dot{n}_b^h = [\frac{f}{1-f}][-n_b^h\lambda_h + n_b^q\lambda_q + n_b^h\frac{\dot{f}}{f}] - n_b^h\frac{\dot{V}(t)}{V(t)}, \tag{4.11}$$

where dot denotes the rate of change of the baryon density with time and λ_q, λ_h are characteristic baryon transfer rates [64] from the QGP to hadron phase and hadron to QGP phase respectively. The definitions of these two quantities are discussed below. $V(t)$ is the volume of the region under consideration. The term $\frac{\dot{V}(t)}{V(t)}$ arises due to expansion of the universe and is given by

$$\frac{\dot{V}(t)}{V(t)} = 3\frac{\dot{R}(t)}{R(t)}. \tag{4.12}$$

Now in our model, each cosmic string forms wake like overdensity leading the trapping of the QGP region in between two planar interfaces. Collapse of these two interfaces towards each other leads to the concentration of baryons which is the subject of study here. Numerical simulations have shown that in the scaling regime, there are $(10-15)$ strings [79] per horizon. For any reasonable GUT scale, strings are definitely in the scaling regime by the stage of the quark hadron phase transition epoch. Initial time relevant for us is the stage when planar interfaces have formed (by coalescence of hadronic bubbles in the regions in between the wakes of different

strings) at the two boundaries of overdense wakes. At this stage, we take the initial volume relevant for each string as,

$$V_0 \approx (\frac{1}{15})\, r_H^3 \tag{4.13}$$

where $r_H(=2t)$ is the size of the horizon at this initial time t_0. Note that we take the wake like overdense regions to be well formed at the time t_0. We take the simple picture that baryon concentration in each such volume is determined by the collapse of two interfaces at the boundary of wake of a single string, without getting significantly affected by the presence of wakes in the region outside the relevant comoving region. As mentioned earlier, this approximation should be o.k. for determining the order of magnitude of baryon overdensities etc. Thus our representative volume is, $V(t) = V_0(\frac{R(t)}{R_0})^3$.

Now let us define the terms $n_b^q\lambda_q$ and $n_b^h\lambda_h$ which appear in the transport rate equations Eq.(4.10) and Eq.(4.11). In our model the interface of the QGP region inside the string wake consists of two planar sheets. (This is in contrast to the situation in ref.[64] where the interface was a spherical surface). The area of each interface sheet is $A \sim V(t)^{2/3}$, assuming the planar interface extending over the region with volume $V(t)$. $n_b^q\lambda_q$ in ref.[64] is defined as the total baryon number swept by the sheets in the overdense region, and pushed through the underdense region, divided by the total volume in the overdense region which is $f(t)V(t)$. Recall that $f(t)$ is the fraction of the volume in the QGP phase. We get,

$$n_b^q\lambda_q = \frac{2A(\frac{dz}{dt})Fn_b^q}{fV(t)}. \tag{4.14}$$

Here, F is a filter factor which we will discuss below. $(\frac{dz}{dt}) \equiv v_z$ is the speed of the interfaces. The factor 2 in the right hand side arises due to the fact there is a pair of sheets bounding the QGP region, which are collapsing towards each other. We write Eq.(4.14) as,

$$n_b^q \lambda_q = \frac{2V(t)^{\frac{-1}{3}}(v_z)Fn_b^q}{f}. \tag{4.15}$$

Similarly, $n_b^h \lambda_h$ is defined as [64],

$$n_b^h \lambda_h = (\frac{1}{3})(\frac{n_b^h v_b \Sigma_h}{f})(\frac{2A}{V(t)}) \tag{4.16}$$

$$= (\frac{2}{3})(\frac{n_b^h v_b \Sigma_h}{f})V(t)^{(\frac{-1}{3})}. \tag{4.17}$$

Here, Σ_h is the baryon transmission probability across the phase boundary from the hadron phase to the QGP phase, and $v_b \simeq (3T/m)^{1/2}$ is typical thermal velocity of baryons in the hadron phase. m is the mass of a nucleon. In these equations, baryon transmission across the interface is characterized by two parameters, F (from QGP to hadronic phase), and Σ_h (from the hadronic phase to the QGP phase). Determination of these parameters does not depend on the geometry of the interfaces, which is the main difference between our model and the one discussed in ref.[64]. For the sake of completeness, we reproduce below some of the steps from ref.[64] for the determination of F and Σ_h.

We start with the number density of the quarks as [2],

$$n_q \simeq 0.3gaT^3, \tag{4.18}$$

where, $g = 2n_f n_c$ is the statistical weight, and n_c, n_f are the number of colors and the number of flavors respectively. Following the phase-space arguments the recombination rate per unit area of the quark as it approaches towards the interface separating the two phases has been defined in ref.[64] as,

$$\Lambda \equiv \Phi^q \Sigma_Q, \tag{4.19}$$

where Φ^q is the net flux of quarks and Σ_Q is the probability of combining three quarks at the front into a color singlet, which can be estimated as [64],

$$\Sigma_Q = (1.4 \times 10^{-5})\Sigma_q[\frac{T}{100 \text{ MeV}}]^9, \tag{4.20}$$

where Σ_q characterizes the probability of transmission across the phase boundary. From Eq.(4.19) and Eq.(4.20) we get the total baryon recombination rate across the boundary [64] as

$$\Lambda \approx (3.3 \times 10^{42})[\frac{T}{100 \text{ MeV}}]^{12}\Sigma_q(\text{cm}^{-2}\text{s}^{-1}), \tag{4.21}$$

where Eq.(4.18) has been used for the net flux of quarks. If we define ξ as the ratio of the net number of baryons over antibaryons to the total number of baryons, then,

$$\xi \equiv \frac{n_b - n_{\bar{b}}}{n_b^{tot}} \approx \frac{0.61\mu_b}{T}, \tag{4.22}$$

where the net baryon number density $(n_b - n_{\bar{b}}) = \frac{n_c n_f}{27}T^3(\frac{\mu_b}{T})$. Therefore, the net baryon transport rate is given by [64] $\Lambda_q = \Lambda\xi$, i.e.,

$$\Lambda_q \simeq (2 \times 10^{42})\Sigma_q[\frac{T}{100 \text{ MeV}}]^{12} \times [\frac{\mu_b}{T}](\text{cm}^{-2}\text{s}^{-1}). \tag{4.23}$$

The filter factor F in Eq.(4.14) is defined as the ratio of the net baryon number (ΔN_b) recombined to the net number of baryons encountered (N_b) at the front per unit area in time Δt. With v_z being the front velocity, the expression of N_b is given as

$$N_b(\text{cm}^{-2}) = (n_b - n_{\bar{b}})v_z\Delta t. \tag{4.24}$$

Similarly the expression of (ΔN_b) can be written as

$$\begin{aligned}\Delta N_b(\text{cm}^{-2}) &= \Lambda_q \Delta t \\ &\simeq (2 \times 10^{36})\Sigma_q[\frac{T}{100 \text{ MeV}}]^{12} \times [\frac{\mu_b}{T}][\frac{\Delta t}{10^{-6}s}].\end{aligned} \tag{4.25}$$

So the filter factor F is given by

$$F \equiv \frac{\Delta N_b}{N_b} = (2.3 \times 10^{-6})[\frac{T}{100 \text{ MeV}}]^9 \Sigma_q v_z^{-1}. \tag{4.26}$$

So far we have considered the baryon transport rate from the QGP phase to hadron phase. Following the similar arguments baryon transport rate for the reverse process, i.e. from the hadron phase to the QGP phase, can be calculated as follows. The net flux of baryons directed at the wall from the hadron phase is taken as [64],

$$\Phi^h \approx \frac{1}{3} n_b^h v_b = [\frac{8}{3\pi^3}]^{\frac{1}{2}} T^2 m [\frac{\mu_b}{T}] e^{-\frac{m}{T}}, \tag{4.27}$$

where again m and v_b are the mass and mean velocity of a nucleon. With Σ_h defined above as the probability of a baryon to pass through the phase boundary, we can write baryon transport rate from the hadron phase to the quark - gluon plasma phase as [64]

$$\Lambda_h \approx (1.1 \times 10^{49})[\frac{T}{100 \text{ MeV}}]^2 \times [\frac{\mu_b}{T}] e^{(\frac{-m}{T})} \Sigma_h. \tag{4.28}$$

The value of Σ_h depends upon the detailed dynamics of the phase boundary which can be calculated [80] by using chromoelectric flux tube model. Sumiyoshi et al. [80] have shown that depending upon temperature this value may vary from 10^{-2} to 10^{-3} at the transition temperature $T < 200$ MeV. The ratio of the two quantities Σ_h and Σ_q can be obtained from the detailed balance [64] across the phase boundary for a situation when there is chemical equilibrium between the two phases. For this case, baryon transport rate in both directions are same, (i.e. $\Lambda_q = \Lambda_h$), and one gets,

$$\frac{\Sigma_q}{\Sigma_h} \approx (5.4 \times 10^6)[\frac{T}{100 \text{ MeV}}]^{-10} e^{(\frac{-m}{T})}. \tag{4.29}$$

Using the expression for the filter factor F in terms of Σ_q from Eq.(4.26) and using Eqs.(4.14), (4.16), we can write the equations of the baryon transport rate (Eqs.(4.10-4.11)) in both regions in terms of a single parameter Σ_h as follows:

$$\dot{n}_b^q = 2\frac{V_0^{(\frac{-1}{3})}\Sigma_h}{f}(\frac{R_0}{R(t)})[-(2.3 \times 10^{-6})(\frac{T}{100 \text{ MeV}})^9$$

$$\times\frac{\Sigma_q}{\Sigma_h}n_b^q+\frac{1}{3}v_b n_b^h]-n_b^q[\frac{\dot{f}}{f}+\frac{\dot{3}R(t)}{R(t)}], \tag{4.30}$$

$$\dot{n}_b^h=2(\frac{f}{1-f})\frac{V_0^{(\frac{-1}{3})}\Sigma_h}{f}(\frac{R_0}{R(t)})[(2.3\times10^{-6})(\frac{T}{100\text{ MeV}})^9$$

$$\times(\frac{\Sigma_q}{\Sigma_h})n_b^q-(\frac{1}{3})v_b n_b^h]+n_b^h(\frac{\dot{f}}{1-f})-3\frac{\dot{R}(t)}{R(t)}n_b^h. \tag{4.31}$$

Here R_0 is the initial (when the two planar interfaces at the boundaries of the string wake just start collapsing) scale factor, and $\frac{\Sigma_q}{\Sigma_h}$ is given in Eq.(4.29).

These two equations along with the Eq.(4.7) and Eq.(4.9) have to be solved simultaneously to get the detailed evolution of baryon density in the trapped QGP region inside the string wake as well as in the region outside. Baryon inhomogeneity will be produced as baryons are left behind in the hadronic phase as the interfaces collapse. We now study the profile of the resulting baryon overdensity after the interfaces collapse away. Let $N_q(t)$ be the total baryon number in the QGP region at a particular time t. $N_q(t)$ is related to the baryon density n_b^q as :

$$N_q(t)=n_b^q(t)V(t)f(t). \tag{4.32}$$

Taking center of the wake as the origin and considering motion of the interface along z direction, we can write

$$f(t)V(t)=2A(t)z(t). \tag{4.33}$$

From this we get the evolution of the thickness $z(t)$ as,

$$z(t)=\frac{f(t)}{2}V_0^{(\frac{1}{3})}\frac{R(t)}{R_0}. \tag{4.34}$$

To get the profile of the baryon inhomogeneities, let $\rho(z)$ be the baryon density which is left behind at position z as the interfaces collapse. We get,

$$N_q(z) - N_q(z + dz) = A dz \rho(z), \tag{4.35}$$

where the time dependence of z is given in Eq.(4.34). We get,

$$-\frac{dN_q}{dz} = A\rho(z). \tag{4.36}$$

Thus we finally get the density of baryons $\rho(z)$ left behind by the collapsing interfaces as,

$$\rho(z) = V_0^{(\frac{-2}{3})}(\frac{R_0}{R(t)})^2(-\frac{dN_q}{dz}). \tag{4.37}$$

Note here that derivation of this equation assumes that baryons left behind by the collapsing interfaces remain in the same region of z, and do not diffuse away. On the other hand, the derivation of equations for baryon transport (Eq.(4.30)-Eq.(4.31)) was based on the assumption that baryons in both phases homogenize, so that baryon transport equations can be written only in terms of two baryon densities, one for each phase. If baryons do not homogenize in the hadronic phase (as was assumed for Eq.(4.37)), then it will increase the reverse baryon transport rate, i.e. from the hadronic phase to the QGP phase. This will only increase the baryon inhomogeneity produced. Also, as mentioned above, values of Σ_h are expected to be very small. We find that even with two orders of magnitude increase in the value of Σ_h, the relevant width of the profile of baryon overdensity $\rho(z)$ only increases by one order of magnitude. Thus, within this uncertainty, we will use Eq.(4.37) to determine the baryon inhomogeneity profile. Finally we mention that baryon diffusion length for the relevant overdensities here always remains less than few cm, while the length scales of inhomogeneities of interest to us are at least one order of magnitude larger.

Eqs.(4.7),(4.9),(4.30),(4.31) are numerically solved simultaneously to get the evolution of baryon densities n_b^q, and n_b^h in the two phases for two different values of critical temperature $T_c = 150$ MeV and $T_c = 170$ MeV, and for two values of $\Sigma_h = 10^{-1}$ and $\Sigma_h = 10^{-3}$. Figs.4.1-4.2 show plots of n_b^q for these cases. Resulting profiles of

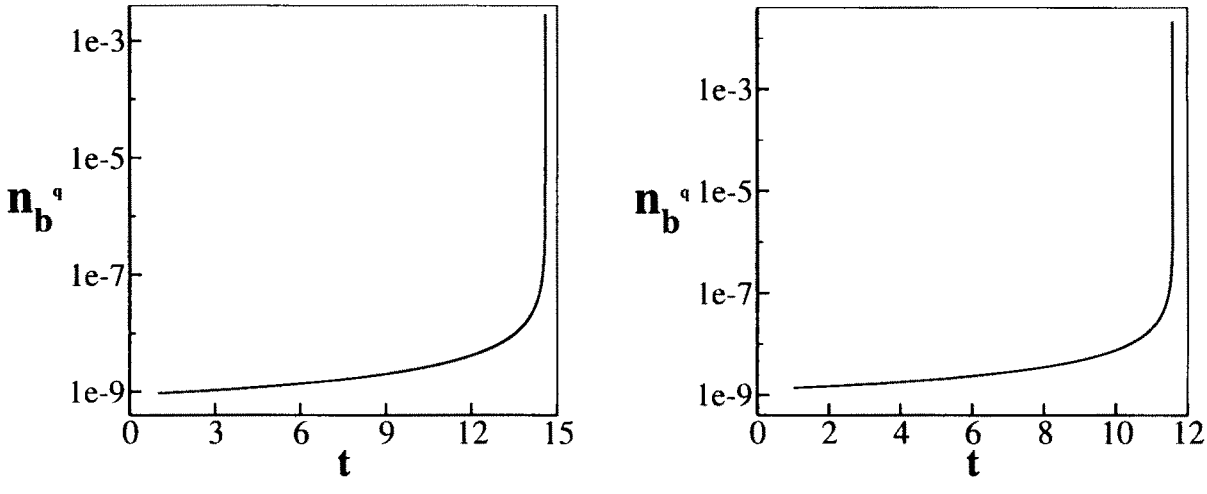

Figure 4.1: These figures show plots of baryon density n_b^q in the QGP phase inside the wake, as a function of time. Σ_h here is 10^{-1}. Left figure is for $T_c = 150$ MeV and right figure is for $T_c = 170$ MeV. Here and in Fig.4.2, n_b^q is in fm^{-3}, while time is given in μs.

baryon overdensity $\rho(z)$ are calculated using Eq.(4.32) and Eq.(4.37), and are shown in Figs.4.3-4.4. Note that in Fig.4.4, there are wiggles in the plot of $\rho(z)$. This is due to numerical errors in calculating $N_q(t)$. As $n_q(t)$ increases, $f(t)V(t)$ decreases, leading to extremely slow variation in $N_q(t)$ for most of the time duration. Thus, as variations in $n_q(t)$ and in $f(t)V(t)$ compensate for each other, the errors become relatively large, as seen in Fig.4.4. We have checked that these errors are in better control for other parameters where the change in $N_q(t)$ is larger. For example, change in N_q will be expected to be larger if Σ_q (which determines baryon transport rate from the QGP phase through the interface to the hadronic phase) is made larger

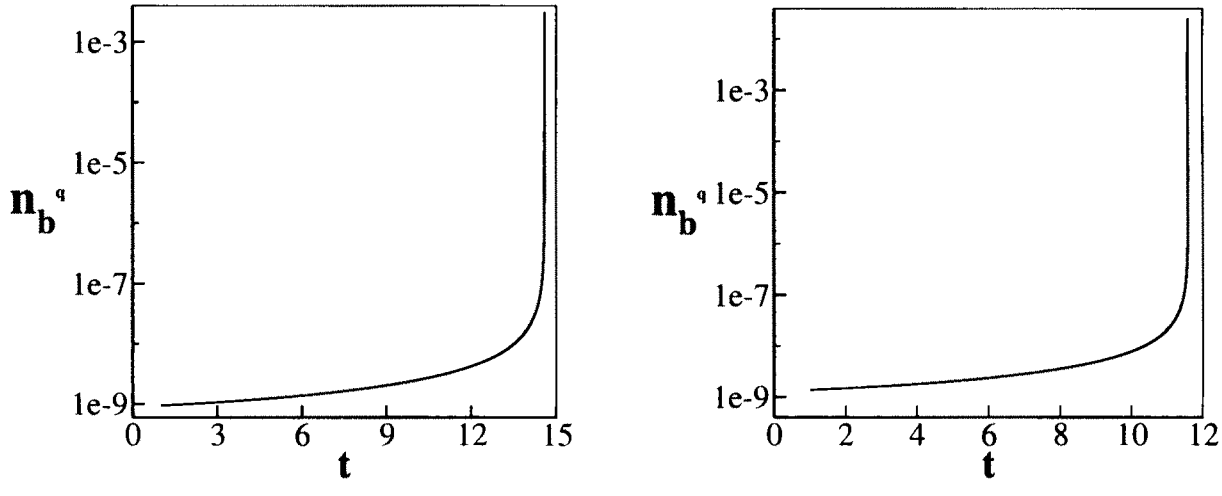

Figure 4.2: Plots of n_b^q as a function of time. Σ_h here is 10^{-3}. Left figure is for $T_c = 150$ MeV and the right figure is for $T_c = 170$ MeV.

while keeping Σ_h (determining baryon transport from hadronic to QGP phase) fixed. This could be achieved by taking the nucleon mass m in Eq.(4.29) to be smaller. We have verified that indeed this happens. For smaller values of m errors become much lower. Of course, as m is not a free parameter, we do not give plots for different values of m. Also, for most of time duration, baryon flow from the QGP phase to hadronic phase dominates over the reverse flow. With m fixed, when Σ_h is increased, Σ_q also increases proportionally via Eq.(4.29). Therefore, a larger Σ_h again leads to a more rapid variation of N_q, giving better control of errors. This can be seen from plots in Fig.4.3 which correspond to $\Sigma_h = 10^{-1}$. No wiggles are seen here, compared to the situation in Fig.4.4 which corresponds to $\Sigma_h = 10^{-3}$.

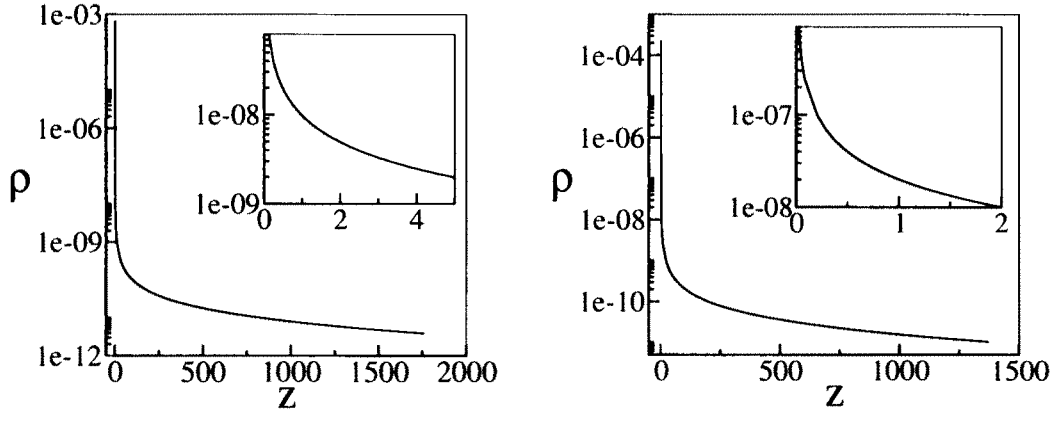

Figure 4.3: These figures show profiles of baryon inhomogeneities $\rho(z)$ generated by collapsing planar interfaces. Σ_h here is 10^{-1}. Top figure is for $T_c = 150$ MeV and the bottom figure is for $T_c = 170$ MeV. Here, and in Fig.4.4, ρ is in units of fm^{-3} while z is given in meters. Insets show expanded plots of the region where ρ becomes larger than 1000 times the asymptotic value. We have estimated the error in numerical evaluation of $\rho(z)$ (here, and in Fig.4.4). Largest error is about 20 % and occurs where wiggles are seen in Fig.4.4. At other parts of plots, error remains below about 5%.

We have used Mathematica routines for numerically solving these coupled differential equations. Due to very wide range of numerical values of various parameters involved, time step for solving differential equation had to be chosen judiciously. For example, for initial times, when distance scale of region in between the interfaces is about 1 km, large values of time step is chosen. As the distance scale decreases, the time step is decreased by factors of 100, ranging from 0.1 μsec to $10^{-9}\mu$sec. This gives a good overall control on the accuracy. An indicator for the error in the numerical solution we obtain is the value of total baryon number $N_t = N_q + N_h$. As the interfaces collapse, converting the QGP phase to the hadronic phase, N_q decreases

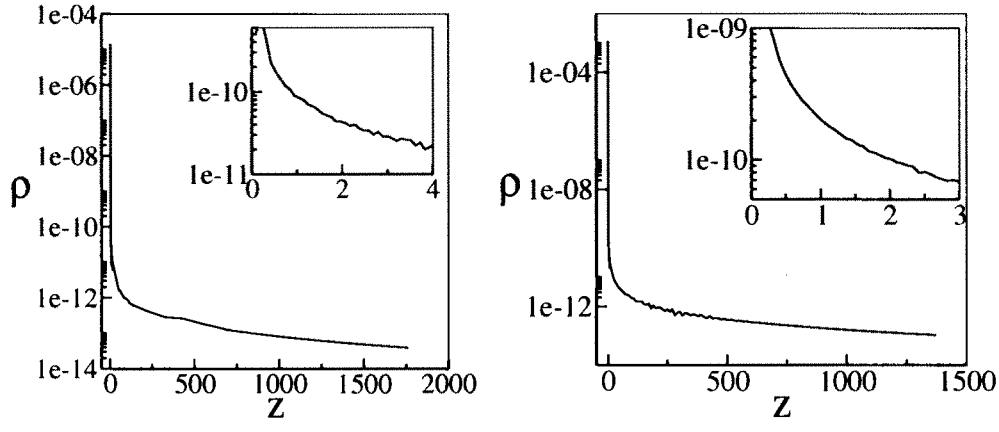

Figure 4.4: Plots of $\rho(z)$ vs. z for the case when Σ_h is 10^{-3}. Top figure is for $T_c = 150$ MeV and the bottom figure is for $T_c = 170$ MeV.

while N_h increases. However, N_t must remain constant. We find that the value of N_t remains reasonably constant over the entire range of integration relevant to us (as shown in Figs.4.3, 4.4). There is a tendency of small net increase in N_t as a function of time. The net increase in the value of N_t (which indicates error in the numerical evolution) remains less than 5% of the net change in the value of N_q over the range of integration in the plots. From Eq.(4.37), we see that the value of $\rho(z)$ is directly proportional to dN_q/dz. Only time dependence in the proportionality factor is in $R(t)$, which changes little over the entire time period, and its evolution is smooth, without any random errors. Similarly, the evolution of $z(t)$ is smooth, without any random errors. Thus, resulting error in $\rho(z)$, as shown in the plots below, should also be less than about 5%. Apart from this error, there is also a random component in the error (again, resulting from extremely slow variation of N_q), leading to random wiggles in the plots of $\rho(z)$ as visible in Fig.4.4. The largest magnitude of this error in

$\rho(z)$ is about 20%. (This error is negligible for plots in Fig.4.3, and also much smaller than 5% at other parts of plots in Fig.4.4 where wiggles are not seen.) As our interest is in order of magnitude estimates of the baryon overdensity (its magnitude, as well as its spatial profile), even the largest possible error of 20% here does not affect our results and conclusions.

As we will discuss in the next section, relevant values of the overdensity n_b'/n_b for us is about 1000. Here n_b' and n_b are baryon densities in the overdense and the background regions respectively. From above plots we see that for $\Sigma_h = 10^{-1}$, the thickness of the region inside which $n_b'/n_b > 1000$ is about 5 meters for $T_c = 150$ and about 4 meters for $T_c = 170$ MeV. For $\Sigma_h = 10^{-3}$ this thickness varies from about 0.5 meters to about 4 meters as T_c changes from 170 to 150 MeV. As baryon density sharply rises for small z, it is more appropriate to calculate the largest value of the width of the inhomogeneity region within which average value of baryon density is 1000 times larger than the asymptotic baryon density. We find that this width is at least an order of magnitude larger than the values mentioned above. For $\Sigma_h = 10^{-1}$ this width is about 100 m for $T_c = 150$ MeV and is about 60 m for $T_c = 170$ MeV. For $\Sigma_h = 10^{-3}$ the values of this width are about 120 m and 90 m for $T_c = 150$ MeV and 170 MeV respectively. As we will see below this type of baryon overdensities can strongly affect abundances of light elements, thereby constraining various parameters of cosmic string models.

4.4 Effect on Nucleosynthesis

With the baryon inhomogeneity profile determined as above at the QCD scale, we need to know the amplitude and length scale of this inhomogeneity at the epoch of nucleosynthesis. For this we use results of ref.[67] where evolution of baryon inhomogeneities of varying amplitude and length scales has been analyzed in detail. From ref.[67] one can see that baryon inhomogeneities of initial magnitude $n_b'/n_b \sim 1000$ at the QCD scale should survive relatively without any dissipation until the stage when

temperature $T \sim 1$ MeV for all the values of length scales relevant for us, i.e. few tens of cm upto about 100 meters. (For example inhomogeneities with baryon to entropy ratio of about 10^{-5} almost do not change during their evolution. Inhomogeneities with larger amplitude eventually dissipate to this value. See, ref.[67].) Though, the length scales in ref.[67] are taken to be comoving at 100 MeV, the results there should apply relatively unchanged for the values of T_c we have considered, i.e. $T_c = 150$ and 170 MeV.

To study the effects of these resulting inhomogeneities at the nucleosynthesis epoch, we use the results of the calculations of the IBBN model developed by Kainulainen et al. [22]. The four crucial parameters in this model are, the average baryon density (η_{avg}), the density contrast ($R \equiv n_b'/n_b$), the volume fraction f_v of the high density region, and the distance scale r of the inhomogeneity at the onset of nucleosynthesis. Out of these, the last three parameters characterize the properties of baryon inhomogeneity regions. We obtain these three parameters from our model and check them with the numerical results in ref.[22] to determine their effects on nucleosynthesis results. Though, the geometry in our case is not exactly the same as the spherically symmetric geometries that have been considered in ref.[22]. However, note that the planar sheet like inhomogeneities of our model should be similar to the geometry of spherical shell (SS) considered in [22]. Therefore, for rough estimates, we will simply take the results of inhomogeneities of the shape of spherical shell from ref.[22], and apply it to our case, making sure of using the corresponding values of the parameters R, f_V, and r.

The results in ref.[22] for the SS geometry were given for a fixed value of $R = 1000$, with f_v varying from about 0.023 to 0.578. In order to be able to use the results of ref.[22], we therefore determine the thickness (and hence the value of f_v) of the baryon inhomogeneity regions from Figs.(4.3)-(4.4) within which $R > 1000$. Again, note that the plots in Figs.(4.3)-(4.4) are given for baryon inhomogeneities at the QCD scale. However, results of ref.[67] show that there is no significant dissipation of these inhomogeneities upto the nucleosynthesis scale. Thus, with length suitably

scaled with the scale factor of the universe, profiles in Figs.(4.3)- (4.4) can be used at the nucleosynthesis stage. We note from Fig.4.3, for $\Sigma_h = 10^{-1}$ that the region of baryon inhomogeneity within which $R > 1000$ has a value of $f_v \simeq 5/2000 \simeq 0.0025$ for both values of $T_c = 150$ and 170 MeV. Here the relevant size of the whole region is taken to be about 2 km. This value of f_v is smaller than the smallest value of $f_v \simeq 0.023$ considered in ref.[22] for the SS geometry case. However, above estimates for f_v are clearly an underestimate as the baryon density is sharply peaked inside the overdense region. As discussed earlier, if we calculate the largest value of the width of the inhomogeneity region inside which the *average* value of the baryon density is 1000 times larger than the asymptotic value then the resulting widths are very large, varying from about 60 meters to about 100 meters. This will then lead to a value of f_v of about 0.03 - 0.05 which are sufficiently large. Note also, that crucial parameter for our case, using which one can determine the order of magnitude effects of baryon density fluctuations on element abundances, is the optimum value of the parameter r. This value depends very weakly on f_v for the SS geometry, with $r_{opt} \sim f_v^{-1/3}$ for $f_v << 1$ (see, ref.[22]). Thus, even with smaller estimates of f_v, the value of r_{opt} relevant for our case will be only about factor 2 larger than the value in ref.[22] for the case $f_v \simeq 0.023$. Similarly, from Fig.4.4 for the case $\Sigma_h = 10^{-3}$, we see that thickness of the inhomogeneity within which $R > 1000$ is about 4 m for $T_c = 150$ MeV, and about 0.5 m for $T_c = 170$ MeV. Corresponding values of f_v are about 10^{-3} and 10^{-4} respectively. In these cases, value of r_{opt} will be increased by about one order of magnitude. Again note that if we take the average baryon density then the relevant width is much larger, about 90 meters to 120 meters. This then leads to a large value of f_v, about 0.045 to 0.06, and hence estimate of r_{opt} remains unchanged. Note also, that in ref.[22] it is mentioned that for maximum effect, the value of Rf_v should be much greater than about 7 (the SBBN proton/neutron ratio at the onset of nucleosynthesis). The smallest value of Rf_v considered in ref.[22] is 23. In our case for smaller estimates of f_v the value of Rf_v is 2.5. However, when we take average baryon density, then the value of Rf_v ranges from about 30 to 60 which is similar to

the values considered in ref.[22].

Next thing we note is that the typical separation between the inhomogeneities, i.e. the parameter r, is about 1-2 km for our case. This corresponds to about 100- 200 km length scale at the nucleosynthesis epoch. Importantly, this is precisely the range of values of r for having optimum effects on nucleosynthesis calculations in ref.[22]. Even with the variations in f_v as discussed above, one can conclude that with $R = 1000$, and with values of f_v corresponding to different cases in Figs.(4.3)-(4.4), the length scales of inhomogeneities in our model (inter-inhomogeneity separation) is roughly in the right range to have optimum effects on nucleosynthesis calculations.

We now apply observational constraints on the abundances of various elements. The most basic constraint is on the abundance of ^{4}He by mass, denoted by Y. If we take a liberal range of values of $Y = 0.238 - 0.244$ (see, ref.[65]), then using the results of IBBN calculations in ref.[22], we see that for inhomogeneities with optimum value of r (which we have argued to be the case here), the corresponding value of η is between about 4×10^{-10} to about 8×10^{-10}. (We mention that most plots in ref.[22] have been given for a different, centrally condensed geometry of the inhomogeneities. However, it has been mentioned there that for SS geometry also results are not too different.) These values are about a factor 2 larger than the allowed values of η for the case of SBBN. (Abundance of ^{7}Li for IBBN models favors somewhat smaller values of η. One needs a careful and detailed comparison of abundances of various elements, ^{4}He, ^{7}Li, and D. However, in view of various uncertainties of our model we will only consider the case of ^{4}He here.)

An independent estimate of η comes from the cosmic microwave background (CMBR) anisotropy measurements. Constraints coming from various experiments seem to constrain η to be less than 6×10^{-10}. If one takes large estimates of ^{4}He, then IBBN calculations suggest that the corresponding value of η will not be consistent with the value obtained from CMBR measurements. Note that SBBN estimates of η for the above range of Y are in very comfortable agreement with CMBR measurements. With this, we conclude that it is suggestive that the baryon inhomogeneities

of the type produced by cosmic strings as discussed above are not consistent with the combined observations of ^{4}He abundance and CMBR anisotropy measurements. Therefore, some of the parameters of the cosmic string model may have to be constrained, so that such inhomogeneities are not produced at the QCD scale. Of course, this is assuming that quark-hadron transition is a first order transition. If the transition is of second order, or a cross-over, (as suggested by many studies), then our calculations do not apply.

If the transition remains of first order, then there are several ways in which production of such inhomogeneities can be avoided. First, if the value of string scale is smaller, say $\sim 10^{15}$ GeV, then from Eq.(3.19) (refer to §3.4.1) we see that resulting value of $\delta\rho/\rho$ will be smaller by one order of magnitude. This implies that the excess temperature inside the string wake region $\delta T/T$ will be about 10^{-6}. This value is much smaller than the value of ΔT_{sc} required for the supercooling for bubble nucleation to start in the outside region. In such a situation, bubble nucleation inside the wake will not be entirely suppressed, though it may still lag behind the nucleation of bubbles in the outside region. Therefore, it is still not excluded that some sort of large scale baryon inhomogeneities will get produced even with string scale of 10^{15} GeV. If this string scale was smaller than 10^{14} GeV, then resulting value of $\delta T/T$ will be even smaller than $\Delta T_n \simeq 10^{-6}$. It is extremely unlikely that in such a case any significant effect will be there on the dynamics of quark-hadron phase transition due to the presence of string wakes.

Yet another possibility is that string velocity is either much smaller, or extremely close to the speed of light. In the first situation, resulting value of $\delta\rho/\rho$ is very small, so no effect will be there on the transition (just as the case for small $G\mu$). For the second situation, when strings move ultra-relativistically, $\delta\rho/\rho$ will be very large (of order 1), so quark-hadron transition dynamics will be strongly affected, producing sheet like baryon inhomogeneities. However, in this case the wake angle θ_w will be very small (of order $8\pi G\mu$). In such a situation, for the region relevant for a single cosmic string, string wake will cover a very small fraction of the total volume. Thus,

when the region outside the wake undergoes hadronization, many localized regions of baryon inhomogeneities will form just as in the conventional models of homogeneous nucleation. Planar interfaces will still form, but they will be able to concentrate baryons from only a very small fraction of the total volume. Thus, resulting baryon inhomogeneities will contribute to negligible baryon fluctuation on the average.

4.5 Conclusion and Discussion

We have calculated the detailed structure of the baryon inhomogeneities created by the cosmic string wakes [14]. We find that the magnitude and length scale of these inhomogeneities is such that they survive until the stage of nucleosynthesis, affecting the calculations of abundances of light elements. A comparison with observational data suggests that such baryon inhomogeneities should not have existed at the nucleosynthesis epoch. If this disagreement holds with more detailed calculations and more accurate observations, then it will lead to the conclusion that cosmic string formation scales above a value of about $10^{14} - 10^{15}$ GeV are not consistent with nucleosynthesis and CMBR observations. Alternatively, some other input in our calculation should be constrained, for example, the average string velocity can be sufficiently small (For relevant value of GUT scale, as strings are not in the friction dominated regime, it may be harder to decrease average string velocity sufficiently.) so that significant density perturbations are never produced at the QCD scale, or strings may move ultra-relativistically so that resulting wakes are very thin, and trap a negligible amount of baryon number. Finally, all these considerations are valid only when quark-hadron transition is of first order.

There are many uncertainties in our model, for example treatment of multiple wakes is rather ad hoc. Also, we have done our analysis for the straight cosmic string case. While discussing the effects of wiggliness on shock formation, we have assumed the simplified picture, namely, the resultant shock for wiggly strings can be obtained by combining the individual shocks produced by each straight segment. The density

fluctuations and opening angle of the wakes, Eq.(4.3) is then derived from Eq.(3.19). However, this treatment is valid when the fluid flow around the string is uniform. In reality, because of the wiggliness of the string the fluid will experience the rapidly changing directions of the wiggles which causes acceleration of the fluid in different direction. So, in proper treatment of shock formation by wiggly string, one should take the non-uniformity nature of the fluid in the analysis.

We have tried to use results from ref.[22] adopting them for our case even though detailed geometry of baryon inhomogeneity in our case is different. A more careful, detailed calculation of abundances of elements is needed for the present case.

The uncertainties in various observations of abundances of elements, as well as CMBR anisotropy will be reduced as precision of various measurements gets better. Then one will be able to say with a greater certainty whether IBBN results puts a strong restriction on the density fluctuations, and hence on cosmic string parameters, or the order of quark-hadron phase transition.